

Correlation between Mechanical and Acoustic Properties of Deformable Metals

M.V. Nadezhkin, S.V. Kolosov, S.A. Barannikova

Institute of Strength Physics and Materials Science, Siberian Branch, Russian Academy of Sciences, Tomsk, Russia

Abstract. In this work, correlations between ultrasonic speed, strength, and plasticity are studied in Fe-18 wt % Cr-10 wt% Ni alloy under uniaxial tension. Special attention is paid to the effect of static loading on acoustic characteristics and destruction parameters of alloy. To provide non-destructive testing of structural state and mechanical parameters of the material under consideration, its acoustic and mechanical properties are finally studied in a temperature range of $180\text{ K} \leq T \leq 318\text{ K}$

Materials and methods. Samples were polycrystalline Fe-18 % Cr -10 % Ni alloys with work piece dimensions of 40x5x2 mm and grain size of $\sim 12.5\ \mu\text{m}$. The uniaxial tensile testing of the specimens was performed on an Instron-1185 universal testing machine at a strain rate of $3.3 \cdot 10^{-4}\ \text{s}^{-1}$. To induce the direct $\gamma \rightarrow \alpha'$ martensitic transformation in the material, the tests were implemented in a temperature range of $180\text{ K} \leq T \leq 318\text{ K}$. The velocity of Rayleigh waves in the alloys was measured using a dual-element sensor consisting of CTS-19 piezoelectric radiating and receiving converters with a resonant frequency of 5 MHz in a housing.

The current study is aimed at establishing the dependences of the ultrasound propagation velocity V and the attenuation coefficient α on the total strain to failure and the tensile strength for the Fe-18 wt % Cr-10 wt % Ni alloy in a wide temperature range

Results. The stress-strain curves of Fe-Ni-Cr alloys cover the ranges of elastic and plastic deformations and fracture. The indicator tension curves initially recorded in the σ (stress)- ε (strain) coordinates were first transformed into the true stress (s)-true strain (e) dependences and then into the destruction diagrams $s(e^{1/2})$ (Fig. 1).

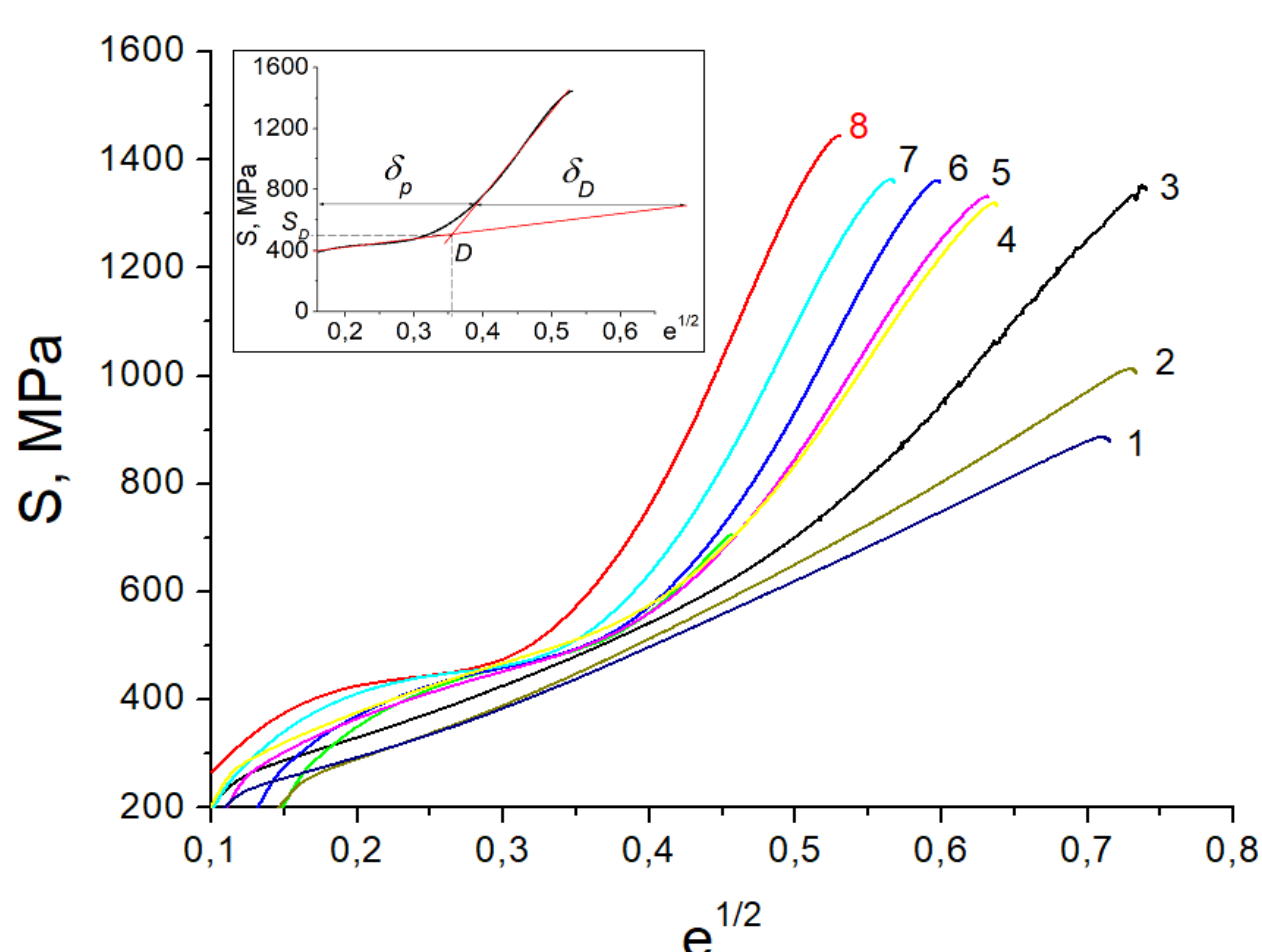


Figure 1 Tension diagrams $s(e^{1/2})$ at temperatures of 334 K (1), 318 K (2), 297 K (3), 270 K (4), 254 K (5), 227 K (6), 211 K (7), 180 K (8).

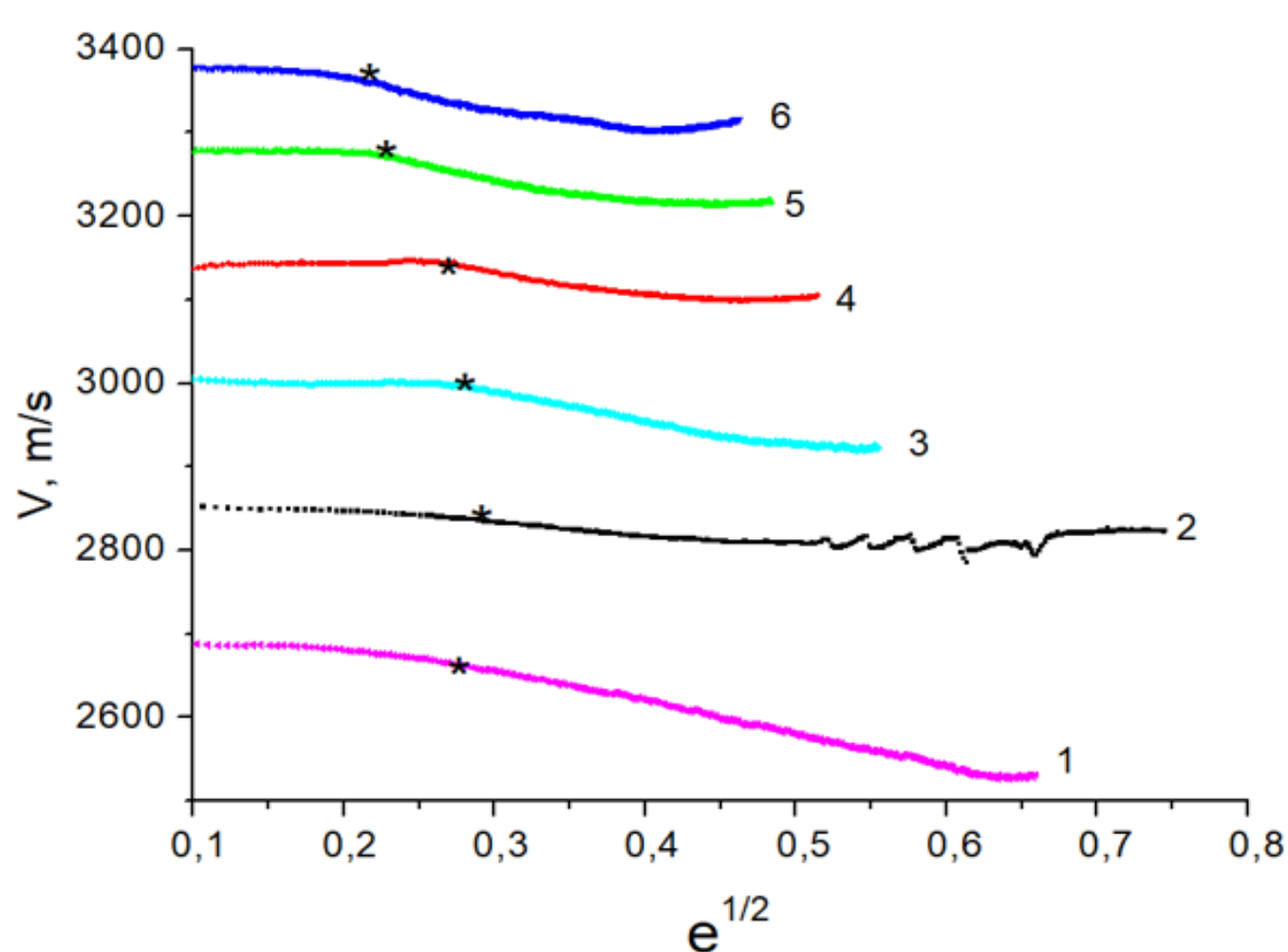


Figure 2 Ultrasound as a function of strain $V(e^{1/2})$ at temperatures of 318 K (1), 297 K (2), 270 K (3), 254 K (4), 211 K (5), 180 K (6).

The samples under tension with decreasing temperature exhibited an increase in their yield strength and ultimate strength and a decrease in the ductility. The linear behavior of the correlation dependences can be qualitatively explained by the functional relationship of the tensile strength σ_B with the elastic properties of the alloy. Indeed, $V = (G/\rho)^{1/2}$, where G is the shear modulus, ρ is the density. Furthermore, the difference of the elastic moduli of the martensite phase released during plastic deformation from those of the material matrix is found to cause the change in the elastic and acoustic characteristics of the entire alloy.

Thus, based on the sound propagation velocity and attenuation in the alloys under consideration, it is possible to predict the ultimate strength and maximum performance of the material at low temperatures. It is obvious that as long as the current deformation is below the value characteristic of point D , the entire total strain is mainly determined by its elasto-plastic component, while the damage-associated component is close to zero. Moreover, during the operation of the unit (product) or pressure treatment, the destruction coefficient remained nonzero, indicating the ability of the material to operate in the plastic-damage stage.

Summary. The analysis of the ultrasound velocity in Fe-Ni-Cr alloys under tension in a wide temperature range of $180\text{ K} \leq T \leq 318\text{ K}$ revealed that a decrease in temperature exerted a significant effect on the ultrasonic wave propagation speed in the materials. The regression dependences were found between various parameters, enabling one to restore certain characteristics based on experimentally determined ones.

As seen from the inset to Fig. 1a the inflection point (referred to as D (destruction) point) in the destruction diagram is attributed to the deformation and strength characteristics (stress S_D and deformation e_D), which can be taken as a criterion of permissible strength ensuring maximum performance of the metal in the studied temperature range. Fixing the destruction points allows one to calculate the destruction coefficient

$$\Delta = \delta_D / \delta_p \quad (1)$$

where δ_p and δ_D are the elasto-plastic and plastic-damage components in the total relative residual deformation (inset in Fig. 1).

Fig. 2 (curves 1-6) displays the ultrasound propagation velocity as a function of total deformation $V(e^{1/2})$, where destruction points are marked as * in accordance with Fig. 1. An increase in the dislocation density and in the martensitic phase volume with a decrease in temperature led to an increase in local internal stresses (stresses of second kind) and eventually to a decrease in the ultrasound velocity.

The analysis of the ultrasound propagation velocity-temperature $V(T)$ plots at each stage of total plastic strain revealed their linear behavior with a correlation coefficient $R = 0.97$. A decrease in the temperature from 297 to 180 K caused a change in the ultrasound velocity $(V-V_0)/V_0$ by 18% in the undeformed sample and by 16% in the deformed one (with a total deformation $e = 0.3$), where V_0 is the speed of sound in the undeformed material at room temperature.

Fig. 3 depicts the temperature dependences of the ultrasound attenuation coefficient $\alpha(T)$ (curve 1), corresponding to the destruction point, and the destruction coefficient $\Delta(T)$ (curve 2). It is established that, in deformable samples, the ultrasound attenuation coefficient behaves as a sigmoid function of tensile strength $\alpha(\sigma_B)$ (Fig. 4), while the ultrasound velocity-tensile strength $V(\sigma_B)$ plot is linear in the studied temperature range.

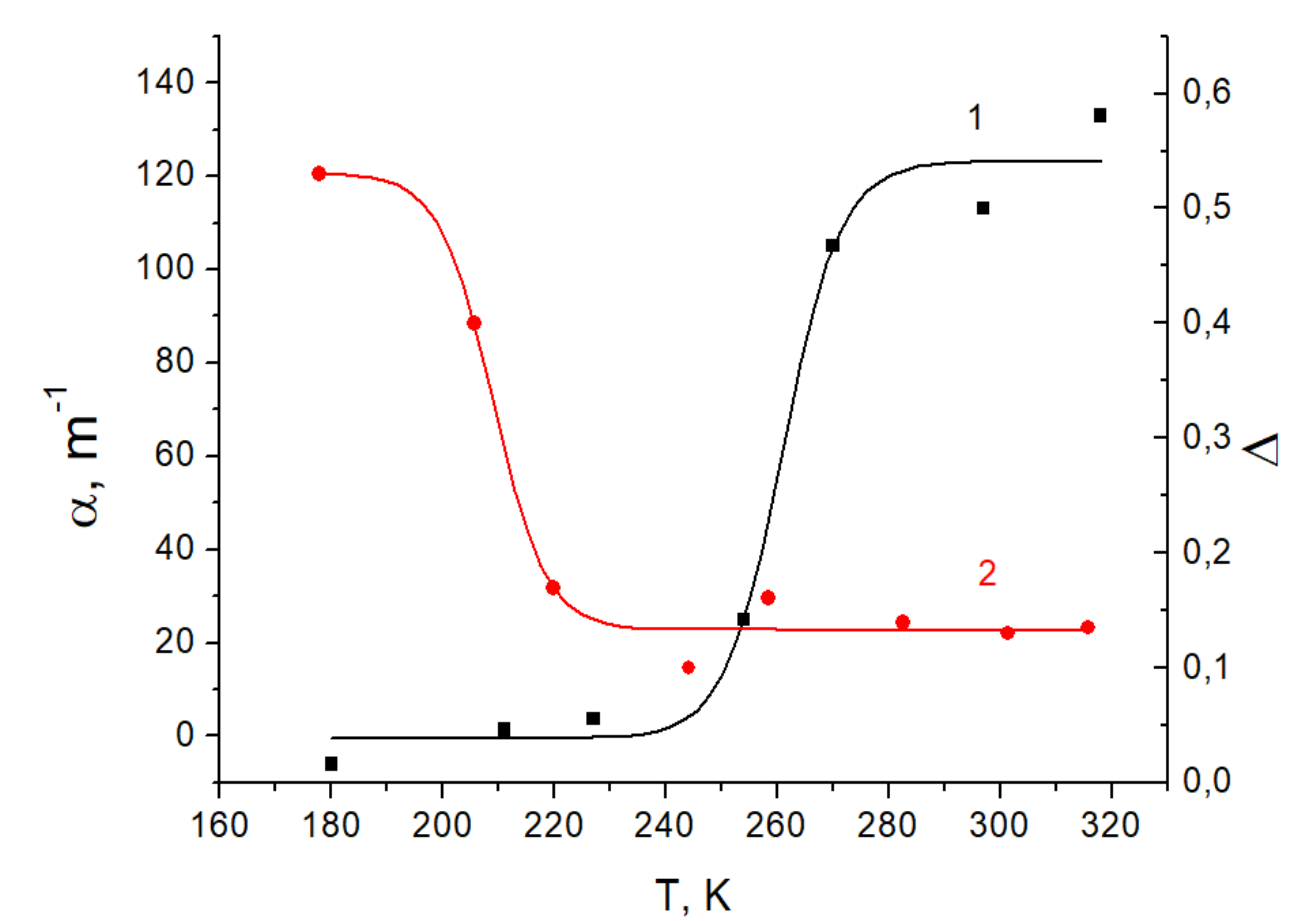


Figure 3 Temperature dependences of ultrasound attenuation coefficient (curve 1) and destruction coefficient (curve 2).

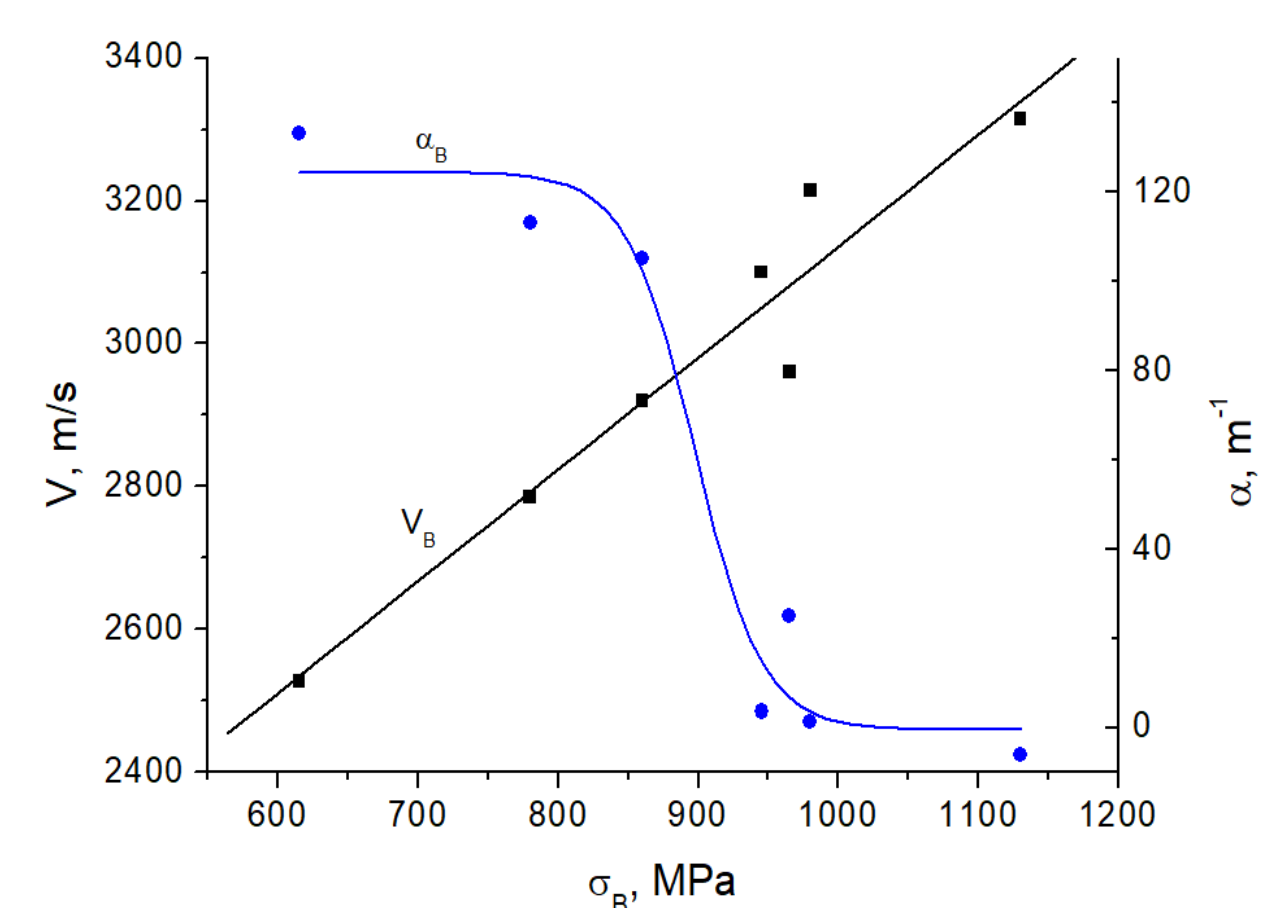


Figure 4 Attenuation coefficient α and ultrasound speed V vs. yield strength σ_B .